

DOI: 10.1002/((please add manuscript number))

Article type: Communication

Charge Carrier Balance for Highly Efficient Inverted Planar Heterojunction Perovskite Solar Cells

Ke Chen,[†] Qin Hu,[†] Tanghao Liu,[†] Lichen Zhao, Deying Luo, Jiang Wu, Yifei Zhang, Wei Zhang, Feng Liu, Thomas P. Russell, Rui Zhu,^{} and Qihuang Gong*

K. Chen, Q. Hu, T. Liu, L. Zhao, D. Luo, J. Wu, Y. Zhang, Prof. R. Zhu, Prof. Q. Gong
State Key Laboratory for Artificial Microstructure and Mesoscopic Physics, School of
Physics, Peking University, Beijing, 100871, China

Q. Hu, Prof. R. Zhu, Prof. Q. Gong

Collaborative Innovation Center of Quantum Matter, Beijing, 100871, China

Dr. W. Zhang

School of Chemistry, Joseph Banks Laboratories, University of Lincoln, Beevor Street,
Lincoln LN6 7DL, United Kingdom

Q. Hu, Prof. F. Liu, Prof. T. P. Russell

Materials Sciences Division, Lawrence Berkeley National Laboratory, CA, 94720, USA

Prof. F. Liu

Department of Physics, Shanghai Jiao Tong University, 200240, Shang Hai, China

Prof. T. P. Russell

Department of Polymer Science and Engineering, University of Massachusetts, Amherst,
MA 01003, USA

Prof. R. Zhu, Prof. Q. Gong

Collaborative Innovation Center of Extreme Optics, Shanxi University, Taiyuan,
Shanxi, 030006, China

* Email: iamzhurui@pku.edu.cn (R. Zhu)

[†] These authors contributed equally.

Keywords: Charge Carrier Balance, Perovskite Solar Cells, Inverted Planar Heterojunction, Highly Efficient, Interface Engineering

Abstract: Perovskite solar cells have attracted tremendous attention in recent years due to the high device performance and the unique optoelectronic properties of perovskite materials. Charge carrier balance is critical for high performance perovskite solar cells. To improve the balance, charge carrier transport process can be manipulated by interface engineering. Here, we report the solvent-treated PEDOT:PSS and additive-modified PCBM as the hole and electron selective contacts, respectively, resulting in accelerated and balanced charge carrier transport within the device. As a consequence, charge carrier accumulation and recombination at the perovskite/selective contact interfaces were suppressed, leading to a power conversion efficiency of 18.72% for a champion cell with a stabilized power output of 17.70% at the maximum power point. We demonstrated that the cells showed negligible current density-voltage (J - V) hysteresis.

Perovskite solar cells (PSCs) have attracted tremendous attention in both the academic and industrial sectors, due to the high device performance, low cost and ease of processability.^[1-4] The performance of PSCs can be significantly limited by charge carrier recombination, due to the unbalanced charge carrier transport in the device.^[5,6] Some effective strategies have been carried out to improve the charge carrier balance, such as: (i) decreasing the bulk recombination losses using a high quality perovskite active layer with long charge carrier lifetimes and diffusion lengths^[7,8] and (ii) increasing the charge carrier collection at the selective contacts by interface engineering,^[9,10] which has led to improved power conversion efficiencies (PCEs).^[11-13]

In the conventional PSCs based on the mesoporous TiO₂, additive doping of TiO₂ has been an effective route to improve charge carrier balance,^[14] since mesoporous TiO₂ provides a large surface area and the charge carriers generated in the perovskite layer can be effectively transported to the electrode by injection into the TiO₂ electron selective contact (ESC) or by the self-connected perovskite network.^[15] In contrast, it is more difficult to balance the hole and electron flux in the p-i-n planar heterojunction (PHJ) PSCs (with a typical structure of ITO/PEDOT:PSS/perovskite/PCBM/top electrode, where the anode is indium tin oxide, ITO, PEDOT:PSS, poly(3,4-ethylenedioxythiophene):poly(styrenesulfonate), is the hole selective contact (HSC) and PCBM is [6,6]-phenyl-C₆₁-butyric acid methyl ester as the ESC) by interface

engineering, due to the limited control of the interface area.^[6,15] Thus far, several methods have been proposed to improved charge carrier balance in the PHJ PSCs by: (i) optimizing the charge carrier selective contacts (*e.g.*, optimization of post annealing process,^[16] modification by additive doping^[17] or utilization of innovative materials^[18]), or (ii) incorporation of multilayer charge carrier selective contacts.^[19,20]

Balanced charge carrier transport is a prerequisite for high performance PSCs.^[7,9] In general, the importance of charge carrier balance has also been demonstrated in polymer solar cells,^[21] light-emitting diodes^[22] and field-effect transistors.^[23] This balance could be effectively improved by engineering the interfaces of the HSC and ESC. As most previous work focused solely on hole or electron selective contact optimization, we aim to provide a simple approach to modify the HSC and ESC simultaneously and demonstrate the correlation of charge carrier dynamics and the device performance.

In this work, we employed the solvent-treated PEDOT:PSS and additive-modified PCBM as the HSC and ESC, respectively. When PEDOT:PSS was rinsed by *N,N*-Dimethylformamide (DMF) and PCBM was modified with 1.0 wt% poly(methylmethacrylate) (PMMA), a significantly enhanced PCE of 18.72% was achieved, in comparison to 16.69% for the reference device. We ascribe the performance enhancement to the accelerated and balanced charge carrier transport from the perovskites to the electrodes, due to HSC and ESC engineering. Using this charge carrier balance strategy, carrier accumulation and recombination were suppressed, based on the

open-circuit photovoltage decay and dark current density-voltage (J - V) results. In addition, the devices with interface engineering showed negligible J - V hysteresis.

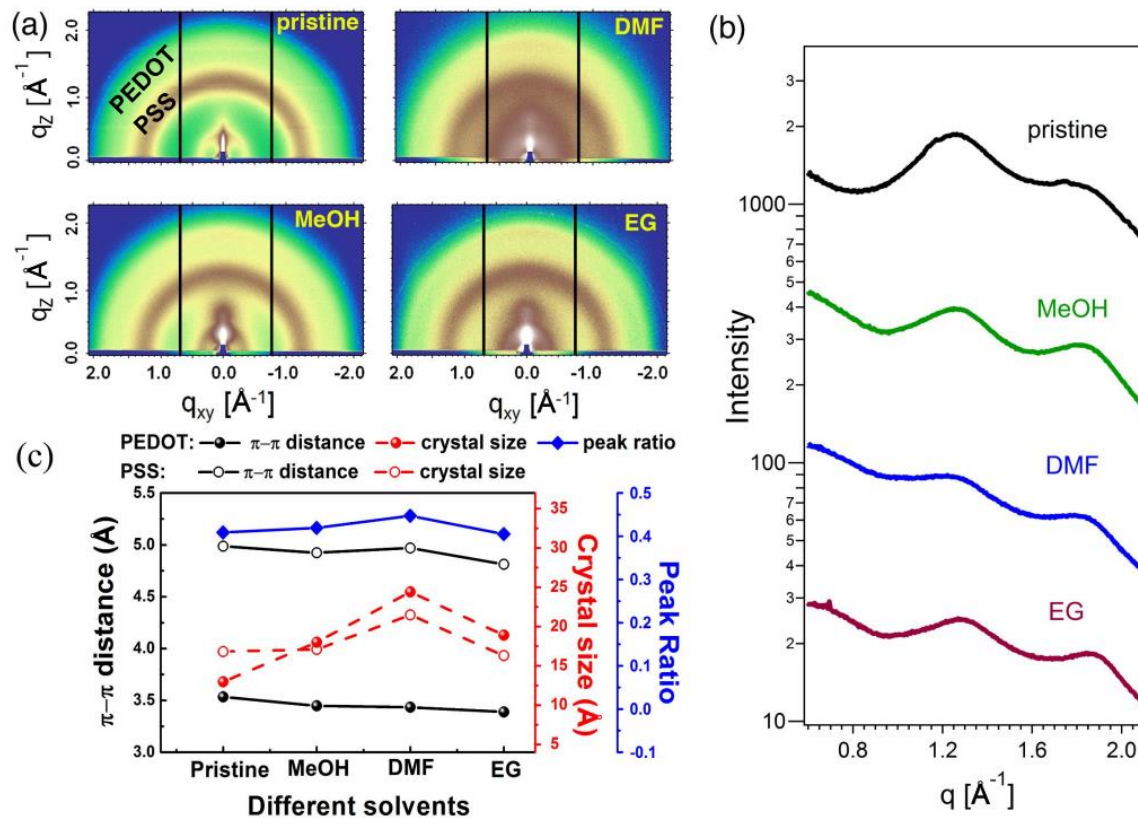


Figure 1. (a) 2D GIWAXS measurements of PEDOT:PSS films treated by different solvents. (b) Sector integrals of the 2D GIWAXS data. (c) An overview of the crystallite sizes, stacking distances, and the PEDOT ratios in PEDOT:PSS films treated by different solvents.

Figure 1a shows the 2D grazing incidence wide-angle X-ray scattering (GIWAXS) images of the as-cast PEDOT:PSS and those from PEDOT:PSS after annealing with methanol (MeOH), DMF, and ethylene glycol (EG). In Figure 1a, the inner and the outer

ring correspond to the scattering from PSS and PEDOT, respectively. Sector-averaged integrals of the q-space converted 2D GIWAXS images are shown in Figure 1b. In general, there are no sharp crystalline reflections observed and it is, therefore, difficult to extract accurate information on crystal size. Using the reflections observed we can determine stacking distances from the centroid of the reflections, an estimate of the relative amounts of PEDOT in PEDOT:PSS, and a very rough estimate of the crystal size, fitting the profiles with Gaussian functions and using a Scherrer analysis.^[24] These are shown in Figure 1c and in Table S1 (Supporting Information). The GIWAXS results for PCBM were essentially invariant after the addition of PMMA (Figure S1, Supporting Information), indicating that the packing of PCBM remains unchanged. The PEDOT crystal size varied from 1.30 nm (as-cast film) to 1.80 nm (MeOH-treated) to 1.89 nm (EG-treated) to 2.44 nm (DMF-treated). Any changes in the apparent crystal size could be attributed to the diffusion of the organic solvent into the PEDOT:PSS and promoting further order.^[24]

Since PEDOT is conductive, while PSS is insulating, the π - π distance of PEDOT (the second maximum in Figure 1b) and the volume fraction of PEDOT could also influence the conductivity of PEDOT:PSS. This distance decreased to 3.45 Å for MeOH, to 3.43 Å for DMF and to 3.39 Å for EG-treated PEDOT:PSS, in comparison to 3.53 Å for the as-cast film. The decrease in the π - π stacking distance results from a interchain coupling of the PEDOT molecules.^[25] The solvent-treated PEDOT:PSS film had a larger

fraction of PEDOT (up to 0.45 for DMF) due to a decrease in the dissociation of PSSH (polystyrene sulfonic acid) into PSS, resulting in less Coulombic interactions with PEDOT.^[26] Hence, a small fraction of PSS can actually be removed when the film is treated with solvents, leading to increased PEDOT ratio in PEDOT:PSS.

In brief, DMF-treated PEDOT:PSS film possesses the largest PEDOT crystalline size and PEDOT ratio, while the EG-treated sample has the smallest π - π stacking distance. The enlarged PEDOT crystallite size, enhanced PEDOT interchain coupling together with increased PEDOT ratio could lead to the conductivity enhancement of PEDOT:PSS.^[24] The conductivity of DMF-treated PEDOT:PSS ($\sim 10^{-1}$ S \cdot cm $^{-1}$) was between the MeOH-treated ($\sim 10^{-2}$ S \cdot cm $^{-1}$) and EG-treated films ($\sim 10^0$ S \cdot cm $^{-1}$), and all have a higher conductivity than the as-cast film ($\sim 10^{-3}$ S \cdot cm $^{-1}$).

Table 1. Photovoltaic parameters summary of PSCs with PEDOT:PSS treated by different solvents, and PCBM modified with different concentrations of PMMA simultaneously with DMF-treated PEDOT:PSS.

HSC/ESC		V_{oc} (V)	J_{sc} (mA\cdotcm$^{-2}$)	FF	PCE (%)
	pristine	0.98	21.83	0.78	16.69
PEDOT:PSS treatment	MeOH	0.98	22.29	0.80	17.48
	DMF	0.98	22.70	0.81	18.02
	EG	0.95	22.96	0.75	16.36

	0%	0.98	22.70	0.81	18.02
PMMA concentration (wt%)	0.5%	1.00	22.49	0.82	18.44
	1.0%	1.02	22.38	0.82	18.72
	1.5%	1.01	22.02	0.81	18.01
	2.0%	0.99	21.57	0.79	16.87

Enhanced conductivity of HSC is conducive to the increased current densities of PSCs (with the structure of ITO/PEDOT:PSS/CH₃NH₃PbI₃/PCBM/BCP/Ag, BCP is bathocuproine as the cathode interfacial layer^[20]). This was confirmed by the photovoltaic results, as shown in **Table 1**. All the solvent-treated devices had higher PCEs than the reference one (PCE = 16.69%). The device with DMF treatment possessed the highest PCE (up to 18.02%). This suggests that DMF is the optimal solvent to treat PEDOT:PSS, in comparison to MeOH and EG. It should be noted that, the work function of PEDOT:PSS is essentially invariant (~5.12 eV, Figure S2, Supporting Information). Thus, the PCE enhancement arises mainly from the improved conductivity (consequently, increased short-circuit current density (J_{sc})) and fill factor (FF).

However, reduced open-circuit voltages (V_{oc}) and FFs were observed for EG-treated devices regardless of higher conductivity (slightly improved J_{sc}) than the DMF-treated samples. With the exception of the increased conductivity, this may arise from the rough surface of the PEDOT:PSS films after EG treatment (Figure S3, Supporting Information). The root mean square (RMS) roughness derived from atomic force microscopy (AFM) is

~2.53 nm in comparison to ~1.98 nm (shown in **Figure 2a**) for the pristine PEDOT:PSS film. The rough surface of PEDOT:PSS could create sharp traps, resulting in surface charge carrier recombination. As a result, a low V_{oc} and FF are expected.^[27] The RMS roughness of the DMF-treated sample decreased to ~0.76 nm (Figure 2b). The smoother surface of PEDOT:PSS could facilitate the interfacial contact between the HSC and the perovskite layer, resulting in a high V_{oc} and FF.^[27,28] As the DMF-treated PEDOT:PSS was the optimized HSC, we used the DMF-treated PEDOT:PSS in this work.

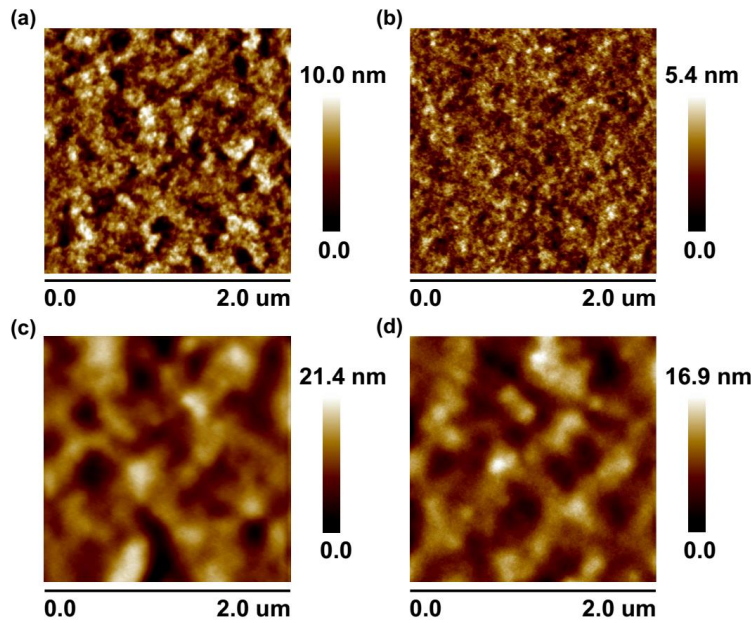


Figure 2. Atomic force microscopy (AFM) images of: (a) Pristine PEDOT:PSS, (b) DMF-treated PEDOT:PSS, (c) Pristine PCBM, (d) PMMA-modified (1.0 wt%) PCBM.

Electron transport between the ESC (PCBM) and perovskite is also important for PCE improvement. However, it is difficult to uniformly coat PCBM on the perovskite

layer, due to the low viscosity of PCBM solution.^[29] Moreover, the aggregation behavior of PCBM could also lead to a poor morphology^[30] and a poor ESC film could easily lead to inefficient electron transport and a decrease in the photovoltaic performance.^[31] To improve the film morphology, we introduced 1.0 wt% PMMA into PCBM to form the PCBM:PMMA hybrid ESC. Figure 2c,d show AFM images of pristine PCBM and hybrid PCBM:PMMA coated onto the perovskite layer. The RMS roughness is ~3.16 nm for the pristine PCBM and only ~2.45 nm for the hybrid film. PMMA helps to increase the viscosity of PCBM solution and suppress the aggregation of PCBM molecules, leading to a uniform ESC film, which should be beneficial for charge carrier collection as we will show in the following discussion.

We optimized the concentration of PMMA based on the DMF-treated PEDOT:PSS. A champion PCE of 18.72% (with a V_{oc} of 1.02 V, J_{sc} of 22.38 mA·cm⁻² and FF of 0.82) was achieved corresponding to the PMMA concentration of 1.0 wt%. The PCE enhancement can be attributed to the increased V_{oc} and FF, which benefit from the improved film morphology.^[15,31] However, further increasing the concentration of PMMA did not improve the device performance, due to the insulating characteristic of PMMA.^[29]

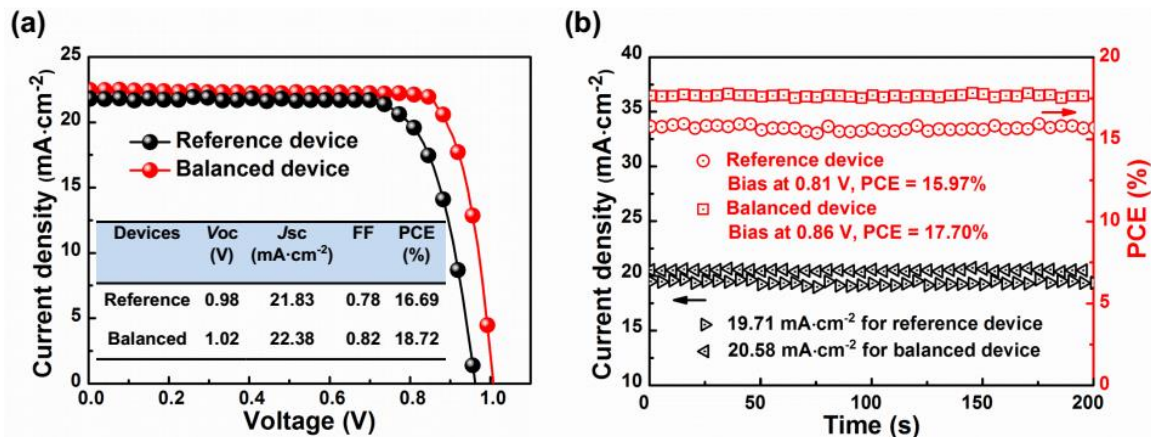


Figure 3. Photovoltaic performance of the reference and balanced device: (a) Current density-voltage (J - V) curves, (b) Steady power output at the voltage near the maximum power point.

Figure 3a shows the J - V curves of the champion device (based on DMF-treated PEDOT:PSS and 1.0 wt% PMMA-modified PCBM, donated as the balanced device) and the reference device (pristine PEDOT:PSS and PCBM). The reference device had a PCE of 16.69% while the balanced device achieved a high PCE of 18.72%. The steady-state photocurrents and efficiencies output were measured at the voltage near the maximum power point, as shown in Figure 3b. The balanced device achieved a stabilized current density of 20.58 mA·cm⁻² and a stabilized PCE of 17.70% at 0.86 V. By contrast, the reference device had a stabilized current density of 19.71 mA·cm⁻² and a stabilized PCE of 15.97% at 0.81 V. Negligible J - V hysteresis was observed in both devices (Figure S4,

Supporting Information). This may be attributed to the passivation effect of the bromide additive on the perovskite trap states.^[32,33]

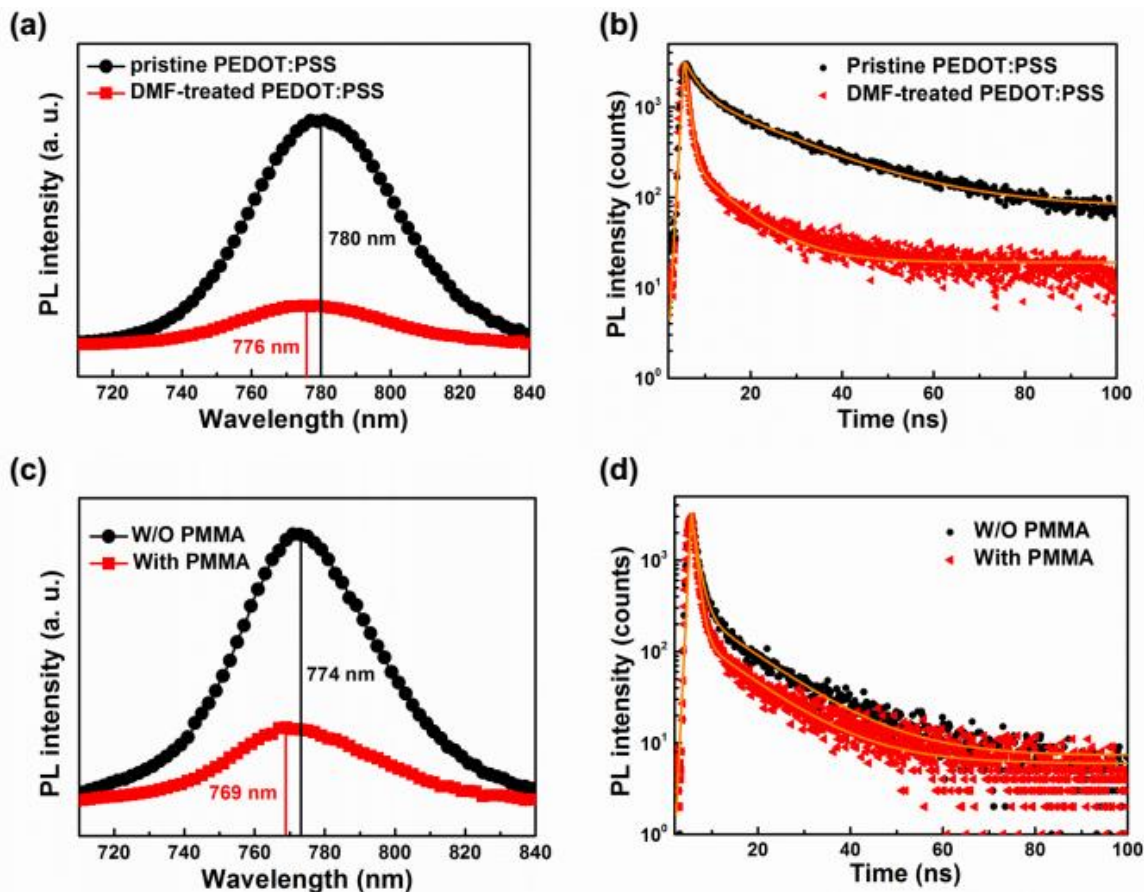


Figure 4. Steady-state photoluminescence (PL) spectra for (a) PEDOT:PSS/perovskite and (c) perovskite/PCBM. Time-resolved PL spectra for (b) PEDOT:PSS/perovskite and (d) perovskite/PCBM.

To understand the superior performance of the balanced device, we studied the charge carrier dynamics through the steady-state and time-resolved photoluminescence

(PL) spectroscopy.^[16,34] **Figure 4a** shows the steady-state PL spectra for PEDOT:PSS/perovskite and PEDOT:PSS(DMF-treated)/perovskite films excited from the ITO side. Figure 4c shows the steady-state PL spectra for perovskite/PCBM and perovskite/PCBM:PMMA films excited from the PCBM side. Blue-shifted PL peaks (from 780 nm to 776 nm at the PEDOT:PSS/perovskite interface and from 774 nm to 769 nm at the perovskite/PCBM interface) were observed. This might be attributed to a decrease of the surface trap states on the interfaces,^[32] since both the HSC and ESC film morphologies were improved after treatment/modification, as shown in Figure 2. Also, the PL intensity of the treated/modified samples showed a stronger quenching effect in comparison to the pristine films. This observation indicates that the DMF treatment and PMMA modification enable better charge carrier collection from the perovskite absorber to PEDOT:PSS and PCBM, respectively.

We further studied the interfacial charge carrier transport process using the time-resolved PL (TRPL) decay measurements. According to the one-dimensional diffusion model,^[9] the observed PL decays were fitted with a bi-exponential decay function containing a fast decay process (indicates the quenching of free carriers through transport to PEDOT:PSS or PCBM) and a slow decay process (indicates the radiative decay).^[35] Figure 4b,d show the TRPL results for the PEDOT:PSS/perovskite and perovskite/PCBM samples, respectively. DMF treatment significantly decreased the fast decay lifetime from 13.62 to 2.95 ns for the PEDOT:PSS/perovskite sample. The same

trend was observed in the perovskite/PCBM film with the fast decay lifetime decreasing from 12.23 to 2.97 ns after PCBM modification with 1.0 wt% PMMA. Reduced fast decay lifetimes suggest faster charge carrier transfer at the interfaces.^[36]

The enhanced charge carrier quenching effect and accelerated charge carrier transport ability were ascribed to the improved conductivity and film morphology of the charge carrier selective contacts. For the PCBM layer, although PMMA is insulating, trace introduction of PMMA could help to suppress the aggregation of PCBM and enhance the interfacial contact with the perovskite,^[29,30] leading to increased electron extraction at the perovskite/PCBM interface.^[15,31] This promoted a more efficient charge carrier collection from the perovskite to the electrode with less energy loss.^[13] It should be noted that, the treated/modified samples had more balanced fast decay lifetimes (2.95 ns at HSC and 2.97 ns at ESC, respectively). This indicates balanced hole and electron extraction abilities at the interfaces.^[35] In addition, the average PL lifetimes (derived from the fast and slow decay lifetime) decreased from 32.25 to 15.74 ns for the PEDOT:PSS/perovskite and from 20.94 to 14.88 ns for the perovskite/PCBM after treatment/modification, leading to balanced PL lifetime ratios (as the perovskite PL lifetime without quencher layer was the same for both samples). This implies balanced hole and electron diffusion lengths according to the one-dimensional diffusion model.^[9,37,38] Balanced charge carrier diffusion lengths in the perovskite and charge carrier extraction abilities at the interfaces could lead to balanced charge carrier transport

in the device, as shown in **Figure 5a**. A balanced transport of holes and electrons is needed to suppress the space-charge formation and the carrier recombination.^[39] The space-charge may result in space-charge limited photocurrents, while the carrier recombination could lead to undesired leakage currents.^[9] They would all negatively affect the device performance.

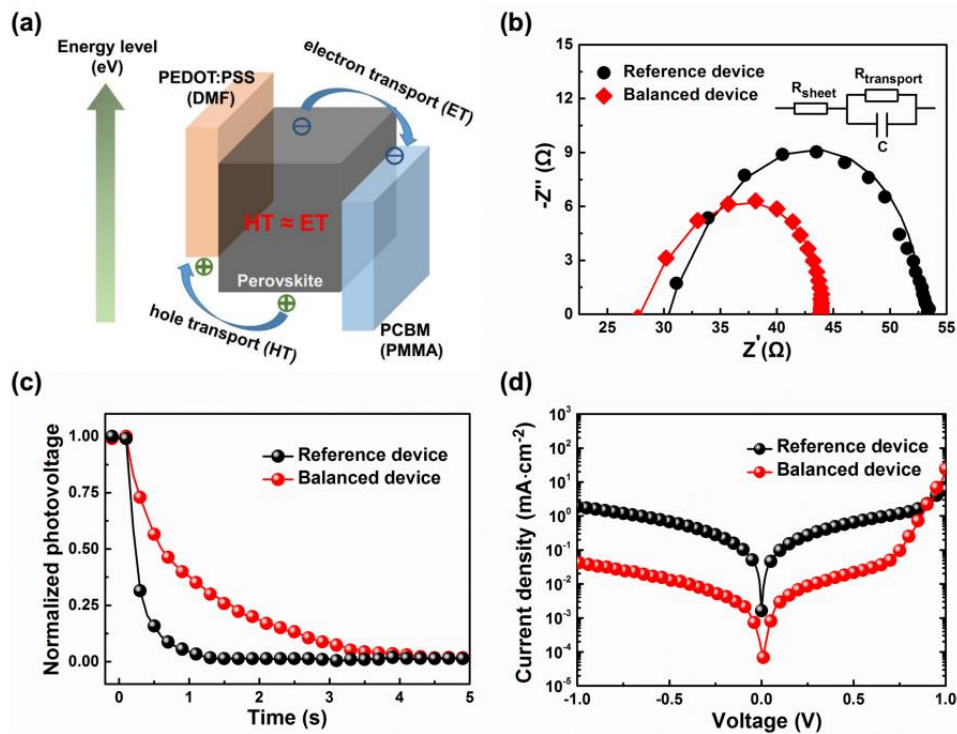


Figure 5. (a) The schematic of charge carrier balance. (b) Nyquist plots of perovskite solar cells. (c) Open-circuit photovoltage decay measurements. (d) Logarithmic plot of $J-V$ characteristics of solar cells measured in the dark.

The PL results show that the charge carrier transport was accelerated and balanced after interface engineering. To understand its influence on the device performance, we further investigated the charge carrier dynamics of the whole cell. Firstly, we performed the impedance spectroscopy (IS) measurement to study the inner series resistances (consist of the sheet resistance R_{sheet} of the cell and the charge carrier transport resistance $R_{\text{transport}}$ at the interfaces) of the devices.^[40] The experiment data were well-described by the equivalent circuit, as shown in the inset of Figure 5b. From the IS modeling, R_{sheet} and $R_{\text{transport}}$ are extracted. The R_{sheet} were 24.3 and 22.0 Ω for the reference and balanced device, respectively. The smaller R_{sheet} of balanced device was ascribed to the increased conductivity of PEDOT:PSS after DMF treatment. The $R_{\text{transport}}$ also dropped from 28.4 (reference device) to 21.9 Ω (balanced device), confirming that the charge carrier transport process was accelerated. This could reduce energy loss during the charge carrier collection, thus boost the device photocurrent and PCE.^[40,41]

We also conducted open-circuit photovoltage decay measurements to understand the balanced charge carrier transport. Here, we monitored the device V_{oc} as a function of time starting from the illuminated steady-state equilibrium to the dark equilibrium. As mentioned above, the unbalanced charge carrier transport would result in the formation of space-charge. Due to the recombination of the space-charge, the V_{oc} would decay.^[29] As shown in Figure 5c, the V_{oc} of the balanced device had a slower photovoltage decay than the reference, suggesting a lower charge carrier recombination rate and, thus, more

balanced charge carrier transport.^[41] Suppressed charge carrier recombination was also confirmed by the dark current measurements,^[31] as shown in Figure 5d. The dark current densities of the balanced devices were almost two orders of magnitude lower than those of the reference ones. This means that more photocurrents would flow through the PSC instead of direct shunting, resulting in suppressed charge carrier recombination and leakage current.^[30]

In summary, we employed the DMF-treated PEDOT:PSS and PMMA-modified PCBM as the HSC and ESC, respectively, to establish charge carrier balance in the inverted PHJ PSCs. The DMF treatment helps to enhance the conductivity of PEDOT:PSS film and reduce its surface roughness, which facilitates the interfacial contact between the perovskite layer and HSC. We also improved the PCBM film morphology by the introduction of PMMA. The interface engineering of HSC and ESC resulted in accelerated and balanced charge carrier transport in the device, leading to the suppressed charge carrier accumulation and recombination. This strategy enables us to achieve a high PCE of 18.72% with a stabilized output efficiency of 17.70% at the maximum power point. This study provides a simple and effective protocol to improve the performance of PSCs based on the interface charge carrier transport modulation.

Experimental Section

Materials: Poly(3,4-ethylenedioxythiophene):poly(styrenesulfonate) (PEDOT:PSS, P VP AI4083) was purchased from Heraeus Clevios. Lead acetate ($\text{Pb}(\text{Ac})_2$) was purchased from Sinopharm Group Company and dehydrated at 50 °C for 48 hours in the vacuum oven before use. Methylamine iodide (MAI) and methylamine bromide (MABr) was synthesized with methylamine (MA) and hydrohalic acid (HX) through the method reported by the previous literature.^[12] [6,6]-phenyl-C₆₁-butyric acid methyl ester (PCBM) was purchased from Nano-C Tech. 2,9-dimethyl-4,7-diphenyl-1,10-phenanthroline (BCP) was purchased from SunaTech Inc. *N,N*-Dimethylformamide (DMF), 2-propanol (IPA), and chlorobenzene (CB), were purchased from commercial sources (Acros) and used as received.

Fabrication of Perovskite Solar Cells: PEDOT:PSS was spin-coated onto a clean ITO substrate (1.5 cm × 1.5 cm, 15 Ω/\square) at 3000 rpm for 30 s and annealed at 130 °C for 20 min in the air. After it was cooled down to room temperature, 60 μL DMF was dropped onto the film for 5s, and then spun off at 3000 rpm for 30 s. Next, MAI and the dehydrated $\text{Pb}(\text{Ac})_2$ were dissolved in anhydrous DMF at a 3:1 molar ratio with 1.0 mol% MABr additive. The precursor solution was spin-coated onto the PEDOT:PSS layer at 4000 rpm for 40 s. And then the compact and well crystallized $\text{CH}_3\text{NH}_3\text{PbI}_3$ films (300 nm) were obtained (shown in Figure S5-7, Supporting Information) after thermal

annealing at 75 °C for 5 min. PCBM (20 mg·mL⁻¹ in CB) solution with 1.0 wt% PMMA additive was spin-coated on top of perovskite layer at 1000 rpm for 45 s to form a hybrid electron collection layer. After that, BCP in IPA was spin-coated at 1000 rpm. Finally, metal silver (80 nm) electrode was thermally evaporated in the vacuum chamber with the pressure of $< 4 \times 10^{-4}$ Pa through a shadow mask.

Characterization of perovskite solar cells: Simulated AM 1.5G irradiation (100 mW·cm⁻²) was produced by a 150 W class AAA solar simulator (XES-40S1, SAN-EI) to irradiate the cells (active area: 0.09 cm²). The light intensity was determined by a standard monocrystalline silicon photodiode calibrated by the Newport TAC-PV lab. A Keithley 2400 source meter was used to measure the *J-V* curves. All samples were measured in a glove box at room temperature without encapsulation.

Other Characterizations: GIWAXS measurements were performed at beamline 7.3.3 at Advanced Light Source, Lawrence Berkeley National Laboratory. The wavelength of X-ray was 1.240 Å, and the incident angle was adjusted to 0.16°. The scattering intensity was detected by a PILATUS 2M detector. The 2D scattering images were analyzed using Nika software package. The FWHM of the peaks, the integrated peak area, and the crystal size were performed using IGOR software. The atomic force microscopy (AFM) images were obtained by the Bruker Dimension Icon in the ScanAsyst mode. Work functions were determined by photoelectron spectroscopy (Rikken Keiki AC-2). The steady-state and time-resolved photoluminescence (PL)

spectra were measured at 767 nm on the excitation at 470 nm by the fluorescence spectrophotometer (FLS980, Edinburgh Instruments, England). The electrochemical impedance spectroscopy (EIS) and open-circuit photovoltage decay measurements were carried out by the electrochemical workstation (Autolab PGSTAT302N, Metrohm, Switzerland). The ESI results were fitted with Nova. The film thickness was measured by stylus profilometry (Bruker Dektak XT). Scanning electron microscopy (SEM) images were obtained by the field-emission SEM (FEI Nova_Nano SEM 430). The X-ray diffraction (XRD) patterns were obtained by Mini Flex 600 (Rigaku, Japan). The ultraviolet-visible (UV-Vis) absorption spectra of the perovskite films were obtained by the spectrophotometer (Agilent 8453, USA).

Supporting Information

Supporting Information is available from the Wiley Online Library or from the author.

Acknowledgements

K.C., Q.H. and T.L. contributed equally to this work. This work was financially supported by the 973 Program of China (2015CB932203), the National Natural Science Foundation of China (61377025, 91433203) and the Young 1000 Talents Global Recruitment Program of China. F.L. and T.P.R. were supported by the U.S. Office of Naval Research under contract N00014-15-1-2244. Q.H. also received support from the Advanced Light Source Doctoral Fellowship in Residence at the Lawrence Berkeley National Laboratory. W.Z. thanks Supergen Supersolar project for support. GIWAXS were performed at beamline 7.3.3 at Advanced Light Source, Lawrence Berkeley National Laboratory, which was supported by the DOE, Office of Science, and Office of Basic Energy Sciences. Work at the Molecular Foundry (Lawrence Berkeley National Laboratory) was supported by the Office of Science, Office of Basic Energy Sciences, of the U.S. Department of Energy under Contract No. DE-AC02-05CH11231.

Received: ((will be filled in by the editorial staff))
Revised: ((will be filled in by the editorial staff))
Published online: ((will be filled in by the editorial staff))

References

- [1] X. Li, D. Bi, C. Yi, J.-D. Décoppet, J. Luo, S. M. Zakeeruddin, A. Hagfeldt, M. Grätzel, *Science*, DOI: 10.1126/science.aaf8060.
- [2] A. Mei, X. Li, L. Liu, Z. Ku, T. Liu, Y. Rong, M. Xu, M. Hu, J. Chen, Y. Yang, M. Grätzel, H. Han, *Science* **2014**, *345*, 295.
- [3] T. Liu, K. Chen, Q. Hu, R. Zhu, Q. Gong, *Adv. Energy Mater.* **2016**, 1600457.
- [4] Y. Zhou, O. S. Game, S. Pang, N. P. Padture, *J. Phys. Chem. Lett.* **2015**, *6*, 4827.
- [5] C. S. Ponseca, T. J. Savenije, M. Abdellah, K. Zheng, A. Yartsev, T. Pascher, T. Harlang, P. Chabera, T. Pullerits, A. Stepanov, J.-P. Wolf, V. Sundström, *J. Am. Chem. Soc.* **2014**, *136*, 5189.
- [6] J. H. Heo, H. J. Han, D. Kim, T. K. Ahn, S. H. Im, *Energy Environ. Sci.* **2015**, *8*, 1602.
- [7] Q. Dong, Y. Fang, Y. Shao, P. Mulligan, J. Qiu, L. Cao, J. Huang, *Science* **2015**, *347*, 967.
- [8] A. Buin, P. Pietsch, J. Xu, O. Voznyy, A. H. Ip, R. Comin, E. H. Sargent, *Nano Lett.* **2014**, *14*, 6281.

- [9] G. Xing, N. Mathews, S. Sun, S. S. Lim, Y. M. Lam, M. Grätzel, S. Mhaisalkar, T. C. Sum, *Science* **2013**, *342*, 344.
- [10] V. W. Bergmann, S. A. L. Weber, F. Javier Ramos, M. K. Nazeeruddin, M. Grätzel, D. Li, A. L. Domanski, I. Lieberwirth, S. Ahmad, R. Berger, *Nat. Commun.* **2014**, *5*, 5001.
- [11] H. Zhou, Q. Chen, G. Li, S. Luo, T.-b. Song, H.-S. Duan, Z. Hong, J. You, Y. Liu, Y. Yang, *Science* **2014**, *345*, 542.
- [12] Q. Hu, J. Wu, C. Jiang, T. Liu, X. Que, R. Zhu, Q. Gong, *ACS Nano* **2014**, *8*, 10161.
- [13] J. Shi, X. Xu, D. Li, Q. Meng, *Small* **2015**, *11*, 2472.
- [14] F. Giordano, A. Abate, J. P. Correa Baena, M. Saliba, T. Matsui, S. H. Im, S. M. Zakeeruddin, M. K. Nazeeruddin, A. Hagfeldt, M. Graetzel, *Nat. Commun.* **2016**, *7*, 10379.
- [15] Z. Zhu, Q. Xue, H. He, K. Jiang, Z. Hu, Y. Bai, T. Zhang, S. Xiao, K. Gundogdu, B. R. Gautam, *Adv. Sci.* **2015**, 1500353.
- [16] Y. Shao, Z. Xiao, C. Bi, Y. Yuan, J. Huang, *Nat. Commun.* **2014**, *5*, 5784.
- [17] W. Chen, Y. Wu, Y. Yue, J. Liu, W. Zhang, X. Yang, H. Chen, E. Bi, I. Ashraful, M. Grätzel, L. Han, *Science* **2015**, *350*, 944.
- [18] C. Sun, Z. Wu, H. L. Yip, H. Zhang, X. F. Jiang, Q. Xue, Z. Hu, Z. Hu, Y. Shen, M. Wang, *Adv. Energy Mater.* **2015**, 1501534.

- [19]O. Malinkiewicz, A. Yella, Y. H. Lee, G. M. Espallargas, M. Graetzel, M. K. Nazeeruddin, H. J. Bolink, *Nat. Photon.* **2014**, *8*, 128.
- [20]D.-X. Yuan, X.-D. Yuan, Q.-Y. Xu, M.-F. Xu, X.-B. Shi, Z.-K. Wang, L.-S. Liao, *Phys. Chem. Chem. Phys.* **2015**, *17*, 26653.
- [21]J. Wang, F. Zhang, M. Zhang, W. Wang, Q. An, L. Li, Q. Sun, W. Tang, J. Zhang, *Phys. Chem. Chem. Phys.* **2015**, *17*, 9835.
- [22]X. Dai, Z. Zhang, Y. Jin, Y. Niu, H. Cao, X. Liang, L. Chen, J. Wang, X. Peng, *Nature* **2014**, *515*, 96.
- [23]Y. Mei, C. Zhang, Z. V. Vardeny, O. D. Jurchescu, *MRS Communications* **2015**, *5*, 297.
- [24]C. M. Palumbiny, F. Liu, T. P. Russell, A. Hexemer, C. Wang, P. Müller-Buschbaum, *Adv. Mater.* **2015**, *27*, 3391.
- [25]N. Kim, B. H. Lee, D. Choi, G. Kim, H. Kim, J.-R. Kim, J. Lee, Y. H. Kahng, K. Lee, *Phys. Rev. Lett.* **2012**, *109*, 106405.
- [26]Y. Xia, J. Ouyang, *J. Mater. Chem.* **2011**, *21*, 4927.
- [27]X. Huang, K. Wang, C. Yi, T. Meng, X. Gong, *Adv. Energy Mater.* **2015**, 1501773.
- [28]Y. Liang, Z. Xu, J. Xia, S.-T. Tsai, Y. Wu, G. Li, C. Ray, L. Yu, *Adv. Mater.* **2010**, *22*, E135.
- [29]Y. Bai, H. Yu, Z. Zhu, K. Jiang, T. Zhang, N. Zhao, S. Yang, H. Yan, *J. Mater. Chem. A* **2015**, *3*, 9098.

- [30]C.-Y. Chang, W.-K. Huang, Y.-C. Chang, K.-T. Lee, C.-T. Chen, *J. Mater. Chem. A* **2016**, *4*, 640.
- [31]F. Xia, Q. Wu, P. Zhou, Y. Li, X. Chen, Q. Liu, J. Zhu, S. Dai, Y. Lu, S. Yang, *ACS Appl. Mater. Interfaces* **2015**, *7*, 13659.
- [32]L. Zhao, D. Luo, J. Wu, Q. Hu, W. Zhang, K. Chen, T. Liu, Y. Liu, Y. Zhang, F. Liu, T. P. Russell, H. J. Snaith, R. Zhu, Q. Gong, *Adv. Funct. Mater.* **2016**, *26*, 3508.
- [33]Y. Zhao, K. Zhu, *J. Am. Chem. Soc.* **2014**, *136*, 12241.
- [34]S. D. Stranks, G. E. Eperon, G. Grancini, C. Menelaou, M. J. P. Alcocer, T. Leijtens, L. M. Herz, A. Petrozza, H. J. Snaith, *Science* **2013**, *342*, 341.
- [35]P.-W. Liang, C.-Y. Liao, C.-C. Chueh, F. Zuo, S. T. Williams, X.-K. Xin, J. Lin, A. K. Y. Jen, *Adv. Mater.* **2014**, *26*, 3748.
- [36]W. Zhang, S. Pathak, N. Sakai, T. Stergiopoulos, P. K. Nayak, N. K. Noel, A. A. Haghighirad, V. M. Burlakov, D. W. deQuilettes, A. Sadhanala, W. Li, L. Wang, D. S. Ginger, R. H. Friend, H. J. Snaith, *Nat. Commun.* **2015**, *6*, 10030.
- [37]S. S. Lim, W. K. Chong, A. Solanki, H. A. Dewi, S. Mhaisalkar, N. Mathews, T. C. Sum, *Phys. Chem. Chem. Phys.*, DOI: 10.1039/c6cp02640k.
- [38]P. E. Shaw, A. Ruseckas, I. D. W. Samuel, *Adv. Mater.* **2008**, *20*, 3516.
- [39]P. W. M. Blom, V. D. Mihailetschi, L. J. A. Koster, D. E. Markov, *Adv. Mater.* **2007**, *19*, 1551.

[40]F. Fabregat-Santiago, G. Garcia-Belmonte, I. Mora-Sero, J. Bisquert, *Phys. Chem.*

Chem. Phys. **2011**, *13*, 9083.

[41]A. Pockett, G. E. Eperon, T. Peltola, H. J. Snaith, A. Walker, L. M. Peter, P. J.

Cameron, *J. Phys. Chem. C* **2015**, *119*, 3456.